electronic reprint

Journal of
Applied Crystallography
ISSN 0021-8898
Editor: **Gernot Kostorz**

Microradian X-ray diffraction in colloidal photonic crystals

A. V. Petukhov, J. H. J. Thijssen, D. C. 't Hart, A. Imhof, A. van Blaaderen, I. P. Dolbnya, A. Snigirev, A. Moussaïd and I. Snigireva

Journal of
Applied Crystallography
ISSN 0021-8898

Received 4 August 2005
Accepted 13 December 2005

Microradian X-ray diffraction in colloidal photonic crystals

A. V. Petukhov,[a]* J. H. J. Thijssen,[b] D. C. 't Hart,[b] A. Imhof,[b] A. van Blaaderen,[b] I. P. Dolbnya,[c]‡ A. Snigirev,[d] A. Moussaïd[d] and I. Snigireva[d]

[a]Van 't Hoff Laboratory for Physical and Colloid Chemistry, Debye Institute, Utrecht University, The Netherlands, [b]Soft Condensed Matter, Debye Institute, Utrecht University, The Netherlands, [c]Swiss–Norwegian Beamline BM-1, ESRF, 38043 Grenoble, France, and [d]European Synchrotron Radiation Facility, 38043 Grenoble, France. Correspondence e-mail: a.v.petukhov@chem.uu.nl

Ultra-high-resolution small-angle X-ray scattering in various colloidal photonic crystals is reported. It is demonstrated that an angular resolution of about two microradians is readily achievable at a third-generation synchrotron source using compound refractive optics. The scheme allows fast acquisition of two-dimensional X-ray diffraction data and can be realised at sample–detector separations of only a few metres. As a result, diffraction measurements in colloidal crystals with interplanar spacings larger than a micrometre, as well as determination of the range of various order parameters from the width of the Bragg peaks, are made possible.

1. Introduction

Suspensions of spherical colloidal particles are able to form close-packed three-dimensional crystals spontaneously at sufficiently high concentration (Pusey & Megen, 1986; Anderson & Lekkerkerker, 2002). Even richer phase behaviour involving various liquid-crystal phases is displayed by colloids of non-spherical shape (Dogic & Fraden, 1997; van der Kooij *et al.*, 2000; Lemaire *et al.*, 2004; Petukhov *et al.*, 2005). This ability to self-organize is extensively used to model crystallization phenomena in atomic and molecular systems. Moreover, colloidal crystals with (sub)micrometre periodicity attract significant attention due to their potential applications as photonic materials (Blanco *et al.*, 2000; Vlasov *et al.*, 2001; Imhof, 2003), which would enable the manipulation of light in a way similar to semiconductors manipulating electrons (Joannopoulos *et al.*, 1995). Despite the significant progress achieved in understanding the various crystal lattices involved (Vos *et al.*, 1997; Sirota *et al.*, 1989; Versmold *et al.*, 2002; Yethiraj & Blaaderen, 2003), the crystallization kinetics (Harland & Megen, 1997; Auer & Frenkel, 2001) and crystal defects (Schall *et al.*, 2004), very little attention has been paid to the long-range order in colloidal crystals (Vlasov *et al.*, 2001; Rengarajan *et al.*, 2005). Compared with other methods, diffraction techniques, which are able to provide detailed macroscopically averaged information, are superior in the quantitative determination of the order parameters over large distances.

Small-angle X-ray scattering (SAXS) has been proven to be a very powerful technique to study the structure of colloidal crystals made of submicrometre particles (Vos *et al.*, 1997; Versmold *et al.*, 2002; Petukhov *et al.*, 2002; Petukhov *et al.*, 2003). In comparison with light scattering (Pusey *et al.*, 1989; Zhu *et al.*, 1997; Harland & Megen, 1997; Kegel & Dhont, 2000), X-rays have an extremely small refractive index contrast (typically of the order of 10^{-6}) and do not require index matching in most cases. SAXS can thus be applied to crystals that are strongly scattering or absorbing in the visible region. Moreover, scattering of X-rays can be measured in a wide range of the scattering vector values q and can therefore be applied to colloidal crystals with periodicities that are too small to be accessed by visible light.

For atomic crystals there are two main types of disorder (Guinier, 1994). In so-called 'perfect' crystals, one finds only disorder of the first type, such as the thermal motion of atoms around the lattice points. It does not disturb the average ideal lattice of the crystal and the positional correlations between the atoms extend over the whole crystal. In 'real' crystals, however, one can also find disorder of the second type, which disturbs the average lattice so that the positional correlations have only a finite spatial extent, smaller than the crystal size. In real colloidal crystals, one can expect that different types of disorder play an important role. In addition to various growth defects, which are also typical for atomic crystals, colloids possess inherent size polydispersity, which can contribute to the disorder of the first type in a colloidal crystal. It can also induce various internal stress fields, which can deform the average lattice and thus can lead to disorder of the second type. The long-range order can be of fundamental importance since it can greatly affect the crystallization rate and influence the size of the grown crystallites. Moreover, disorder of various types can also lead to a significant degradation of the

‡ Present address: Diamond Light Source Ltd, Rutherford Appleton Laboratory, Chilton, Didcot, Oxfordshire OX11 0QX, UK.

performance of the photonic materials fabricated from self-organized colloidal crystals (Astratov *et al.*, 2002; Rengarajan *et al.*, 2005).

Disorder of various types manifests itself in different ways in a diffraction pattern. For small crystals, the finite size effect leads to broadening of the diffraction peaks, which is independent of the diffraction order. In a so-called mosaic consisting of small crystallites, which are orientationaly correlated but positionally independent, the peak width in the azimuthal direction apparently increases with the diffraction order due to small fluctuations in the orientation of different crystallites. However, the radial width is still independent of the diffraction order. The disorder of the first type does not broaden the Bragg peaks but manifests itself in the Debye–Waller factor, which can be accurately measured by SAXS (Megens & Vos, 2001). The disorder of the second type leads to additional peak broadening, which increases with the diffraction order (Guinier, 1994).

The challenge in the application of SAXS for structural characterization of self-assembled colloidal photonic crystals stems from the three to four orders of magnitude difference between the typical size of the colloidal particles and the X-ray wavelength. To resolve the diffraction pattern, one often needs an angular resolution well beyond 10^{-4} radian. Even higher resolution, of the order of 10^{-6} radian, is needed to determine the intrinsic width of the diffraction peaks, which would allow detailed characterization of the long-range order. Moreover, in certain cases (Petukhov *et al.*, 2005) the distinction between different thermodynamic phases can only be made on the basis of the difference in the intrinsic widths of the reflections.

The so-called ultra-small-angle X-ray scattering (USAXS) technique is commonly believed to facilitate the highest angular resolution possible (Narayanan *et al.*, 2001; Ilavsky *et al.*, 2002). It uses a point detector and a set of so-called Bonse–Hart cameras (Bonse & Hart, 1966), each consisting of a pair of Bragg-reflecting crystals. USAXS allows one to resolve the angular spectrum of scattered radiation with a resolution determined by the angular width of the rocking curve of the Bragg reflection. The presently used Si-111 and Si-220 reflections have an angular width of the order of 10^{-5} radian, which is often not sufficient to resolve the intrinsic width of the reflections in colloidal crystals. The resolution of the Bonse–Hart camera can be further enhanced by choosing higher-order reflections (Freund, 1998), but such a possibility has not been realised yet for USAXS applications. More importantly, the USAXS scheme requires a long acquisition time due to its point-by-point data collection. It has been used for samples consisting of a powder of colloidal crystals (Harada *et al.*, 2000), but in the case of single crystals, yielding essentially two-dimensional patterns, the USAXS scheme is very impractical.

Much shorter acquisition time (from minutes down to milliseconds) can be achieved in an ordinary SAXS scheme with a two-dimensional detector. Most of the reported studies of colloidal crystals using a SAXS setup (Vos *et al.*, 1997; Versmold *et al.*, 2002; Petukhov *et al.*, 2002, 2003) were performed with an angular resolution of the order of 10^{-4} radian. A few examples of studies at resolutions of (1–5) $\times$ 10^{-5} radian were also reported for sample–detector distances of the order of 10 m (Linari *et al.*, 2000; Reconditi *et al.*, 2004; Petukhov *et al.*, 2004) and more than 100 m (Yagi & Inoue, 2003). For colloidal crystals with submicrometre lattice spacings, this resolution is sufficient to resolve the Bragg reflections, but the information on the intrinsic width of the reflections can hardly be obtained from the apparent size of the reflections on the detector. Moreover, the resolution of the ordinary SAXS setup is often insufficient for photonic crystals with spacing larger than a micrometre, which are especially interesting for their potential use in near-infrared telecommunication applications (Vlasov *et al.*, 2001).

A significant increase in terms of the angular resolution, well into the 10^{-6} radian range, can be achieved at third-generation synchrotron sources using refractive optics (Drakopoulos *et al.*, 2005). Here we further demonstrate that this gives access to information on long-range order in colloidal crystals, which was not achievable before, and opens up new avenues for future fundamental and applied research.

Throughout the paper, the scattering (diffraction) vector $\mathbf{q} = \mathbf{k}_s - \mathbf{k}_i$ is defined as the vector difference between the wavevector of the scattered $\mathbf{k}_s$ and the incident $\mathbf{k}_i$ waves with $k_s = k_i = 2\pi/\lambda$, where λ denotes the wavelength. The paper is organized as follows. In §2, we briefly review the conditions needed to achieve the high angular resolution. Experimental details are summarized in §3. We then present several examples of our results obtained for various self-organized colloidal crystals. §4 describes the results from a wall-induced crystal of PMMA spheres. In §5, application of the technique to a photonic crystal with interplanar spacing as large as 1.35 μm is demonstrated. A study of disorder of the first and second type in random hexagnal-close-packed (r.h.c.p.) crystals of hard silica spheres is briefly described in §6. The ultimate limit of the angular resolution that can be achieved by the optical setup was measured with high-resolution X-ray films as described in §7. Finally, the results are summarized in §8.

2. Resolution and coherence

An X-ray diffraction pattern originates from interference of waves scattered coherently by colloidal particles. To resolve it, the conditions for constructive interference of coherent waves scattered from particles separated by a few structure periods must be met. To resolve the intrinsic width of the Bragg reflections, one needs coherence over distances that are comparable with the positional correlation length of the structure (Sinha *et al.*, 1998).

In the longitudinal direction, this condition can be easily fulfilled over macroscopic (>100 μm) distances for small diffraction angles (Petukhov *et al.*, 2002, 2004). By tilting the crystal from a certain crystallographic direction and observing the variation of the integrated intensity of reflections, one can achieve a reciprocal-space resolution of the order of $10^{-6}k_i$. This technique, however, is only applicable to single crystals and allows one to measure the intrinsic width of the Bragg

reflections only along the X-ray beam, *i.e.* orthogonal to the scattering vector **q** for a small diffraction angle 2θ. Moreover, one often needs to collect diffraction data for many crystal orientations in order to reconstruct the rocking curve, which requires longer data acquisition times.

Of much more importance is the width of the reflections in the radial direction, along **q**. It can only be probed if a very high angular resolution is achieved. The latter is also much more challenging, since it requires the random fluctuations of the phase front to be much smaller than the tiny X-ray wavelength, λ, on macroscopic distances. For a freely propagating X-ray wave, this condition is fulfilled over the so-called transverse coherence length $l_{\rm trans}$, which is equal to

$$l_{\rm trans} = L\lambda/\sigma, \qquad (1)$$

where σ is the source size and L is the distance travelled by the beam. Furthermore, the beamline optics can affect the beam coherence. Apart from imperfections in the optical elements, which can introduce additional distortions of the phase front, beam focusing can significantly reduce $l_{\rm trans}$ (Petukhov *et al.*, 2004). A simple solution is to avoid beam focusing before the sample and to let it freely propagate to the sample. With a typical source size $\sigma \simeq 100$ µm and the source–sample distance $L \simeq 50$ m at a synchrotron X-ray source, a transverse coherence length of the order of $l_{\rm trans} \simeq 50$–100 µm can be reached, *i.e.* the transmitted X-ray beam will contain information on the positional correlations of the colloidal particles over a distance of about a hundred lattice periods. To extract this information, we have used a compound refractive lens (CRL) (Snigirev *et al.*, 1996), which can recover the Fourier spectrum of the transmitted beam (Kohn *et al.*, 2003) by performing beam focusing onto the detector within a relatively short sample–detector distance (usually limited to several metres by the length of the experimental hutch).

3. Experimental

The experiments were performed at the beamline ID-10A 'TROÏKA III' of the ESRF (Grenoble, France). The fifth harmonic of the undulator source with photon energy of 13.36 keV (wavelength $\lambda = 0.093$ nm) was selected by a flat channel-cut Si-111 monochromator. Due to the particular properties of the electron β-function of the ESRF storage ring, the X-ray source of ID-10 has dimensions of about 25 µm × 1000 µm, *i.e.* it is too large in the horizontal direction to obtain a sufficient coherence length at the sample position. We have therefore used a rather small opening of the primary slits (SS0) of 30 µm in both the horizontal and the vertical directions, as illustrated in Fig. 1. This scheme leads to a significant loss of beam intensity. Fortunately, most of our samples scatter X-rays strongly enough to allow the collection of sufficient signal within short exposure times τ (typically, of the order of a few seconds).

The 30 µm × 30 µm slit sizes were of the order of the transverse coherence length at the position of the SS0 slits in the vertical direction, but about one order of magnitude larger than the transverse coherence length in the horizontal direction. Considering the primary slits as a secondary X-ray source for the rest of the setup, we estimated the transverse coherence length at the sample position to be of the order of $l_{\rm trans} = 100$ µm, and the beam size of a few hundreds of micrometres. Thus, we intentionally did not create the condition for fully coherent X-ray illumination to avoid the appearance of speckle patterns (van der Veen & Pfeiffer, 2004).

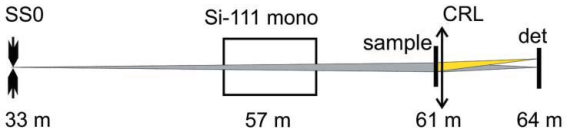

Figure 1
Sketch of the setup. Only the principal components [the primary slits SS0, the Si-111 monochromator, the sample, the lens (CRL), and the detector] are shown. The numbers indicate the distances from the undulator source.

The transmitted and diffracted X-ray beams are focused by a CRL (Snigirev *et al.*, 1996; Drakopoulos *et al.*, 2005) positioned just after the sample. The lens position and its focal length are adjusted such that it creates an image of the secondary X-ray source (SS0) at the position of the detector. For the given SS0–lens and lens–detector distances, the demagnification of the imaging system is about 1:8.5, such that the CRL should produce an image of about 3.5 µm of the SS0 slits of width 30 µm. With the lens–detector distance of $L_{\rm ld} = 3.25$ m, one can therefore expect an angular resolution of the setup of the order of 1 µrad.

The vast majority of the results (§§4–6) are recorded by a 12-bit CCD camera (Sensicam) with a pixel size of 6.7 µm × 6.7 µm and a field size of 8.6 mm × 6.9 mm. The camera was supplemented by an X-ray-sensitive phosphor screen and a 1:1 projecting objective. Since CCD detectors have a rather limited dynamic range (*i.e.* the ratio of maximum to minimum intensity that can be measured reliably at the same instant), every diffraction pattern was recorded several times with different exposure times τ. The shortest exposure is used to quantify the strongest reflections, while the longer exposures were used for analysis of weaker high-order reflections. Furthermore, X-ray-sensitive films (Kodak) with a spatial resolution better than 1 µm are used to probe the angular resolution limit provided by the optical setup as described in §7.

4. Wall crystallization of PMMA spheres

Cylindrical glass capillaries (diameter 1.5 mm, wall thickness 10 µm) were filled with suspensions of poly(methyl metacrylate) (PMMA) colloidal hard spheres in *cis*-decalin at an initial volume fraction of 30%. The particles (diameter 230 nm) are sterically stabilized with 10 nm chemically grafted polyhydrostearic acid. The capillaries were stored vertically to establish a sedimentation–diffusion equilibrium. Visual inspection revealed that the top part of the capillary contained turbid colloidal fluid. Colloidal crystals yielding strong Bragg reflections of visible light formed in the sediment at the bottom of the capillary. Fig. 2(*a*) presents a pattern measured a few millimetres above the crystalline sediment. The broad

rings in the scattering field originate from the fluid phase in the bulk of the suspension. In addition, the sharp Bragg peaks in the pattern reveal that a colloidal crystal had grown at the capillary wall.

The diffraction pattern is typical for an r.h.c.p. crystal. The reciprocal lattice of the r.h.c.p. structure consists of Bragg spots and Bragg rods (Versmold *et al.*, 2002; Petukhov *et al.*, 2003). The stacking-independent Bragg spots are found at the *hkl* reflections with $h - k$ divisible by 3 and with integer values of l. The stacking-disorder-induced Bragg rods with a smooth intensity variation along l are observed for $h - k$ not divisible by 3. For the crystal orientation in Fig. 2(*a*), the X-ray beam is orthogonal to the hexagonal planes and thus $l = 0$. One can clearly see the 110 and 300 reflections originating from the true Bragg spots. Here the contributions from all the hexagonal layers have the same phase leading to a very large structure factor. For $h - k$ not divisible by 3, the contributions of the hexagonal layers possess an additional stacking-dependent phase of 0° or $\pm 120^\circ$, leading to significant cancellation between them and therefore a much smaller structure factor. This explains the significantly weaker diffraction intensity of the 100 reflection relative to the 110 reflection, despite the much larger form factor of the former. Similarly, the 300 reflection is much stronger than the 200 reflection with much higher form factor. The 220 reflection with a strong structure factor is, however, hardly visible since it appears very close to the zero of the form factor.

Panel (*b*) of Fig. 2 presents a magnified ($\times 20$) view of one of the 110-class reflections. For comparison, an image of the direct beam is also given in panel (*c*). By adjusting the exposure time τ, we made sure that the intensity scale was similar in the data presented in (*b*) and (*c*). It is seen that both peaks have practically the same width, *i.e.* the 110 reflection from the colloidal crystal is practically instrument-limited. This is further illustrated in panel (*d*), where the horizontal profiles through both peaks are presented. The pixel intensities were fitted with a Lorentzian line profile. For the profile of the direct beam, which can be considered as the instrument resolution function, the fit yields a full width at half-maximum (FWHM) of $\Delta_{\rm ver} = 3.12 \times 10^{-4}\,{\rm nm}^{-1}$ and $\Delta_{\rm hor} = 3.09 \times 10^{-4}\,{\rm nm}^{-1}$ in the vertical and the horizontal directions, respectively. This means that in angular terms, the digital data recorded with the CCD detector have a resolution of about 4.6 μrad. We will show in §7 that this value is mainly limited by the resolution of the detector.

For the 110 reflection in Fig. 2(*b*), the Lorentzian fits yield an FWHM of $3.87 \times 10^{-4}\,{\rm nm}^{-1}$ and $3.62 \times 10^{-4}\,{\rm nm}^{-1}$ in the vertical and the horizontal directions, respectively. These values are slightly higher than those for the instrument resolution. Since the intrinsic width of the sample reflection $\delta q_{\rm intr}$ and the width of the instrument resolution Δ yield statistically independent contributions to the apparent reflection width $\delta q_{\rm app}$, we may assume that

$$\delta q_{\rm app}^2 = \Delta^2 + \delta q_{\rm intr}^2. \qquad (2)$$

Substituting the obtained widths of the Lorentzian fits, one obtains $\delta q_{\rm intr} = 2.3 \times 10^{-4}\,{\rm nm}^{-1}$ and $1.9 \times 10^{-4}\,{\rm nm}^{-1}$ in the vertical and the horizontal directions, respectively. For comparison, the magnitude of the diffraction vector of the 110 reflection is $q_{110} = 4.70 \times 10^{-2}\,{\rm nm}^{-1}$. It is worth stressing that these values of $\delta q_{\rm intr}$ can only be used as an order-of-magnitude indication of the upper limit of the width of the crystal reflections. The peak profiles of the direct beam and the crystal reflections are very close to each other (Fig. 2*d*) and a small inaccuracy in the determination of their widths can lead to a significant change of $\delta q_{\rm intr}$ due to the relation assumed in equation (2).

5. Photonic crystals with a periodicity larger than a micrometre

In order to open up a photonic band gap, photonic crystals require a large refractive-index contrast for visible and near-infrared light. This complicates characterization of their structure using optical techniques. As X-rays interact relatively weakly with matter, they form an excellent probe for the internal three-dimensional structure and order of photonic crystals. Photonic materials for near-infrared telecommunication applications with spacings of the order of 1 μm are especially challenging for the X-ray scattering technique, because the diffraction angles are extremely small. Here we demonstrate application of SAXS with microradian resolution to such a crystal with a very large period.

The colloidal crystals were made using the method of Yethiraj *et al.* (2004), which allows growth of large colloidal single crystals. Silica colloidal spheres (diameter $d = 1.4$ μm) in a refractive-index-matching solvent mixture of water and dimethyl sulfoxide (DMSO) were allowed to sediment in an electric field perpendicular to gravity. The external electric field adds a long-range dipolar term to the interaction potential of the particles (Yethiraj & Blaaderen, 2003). For high field strengths, the dipolar term dominates, favouring the formation of body-centred tetragonal (b.c.t.) instead of close-packed structures (Dassanayake *et al.*, 2000). The b.c.t. samples consist of AB-stacked hexagonal layers parallel to the glass substrate. However, the layers are bridge-site instead of hollow-site stacked. Using a polymerization process, this metastable b.c.t. structure can be preserved, even after switching the electric field off (Yethiraj *et al.*, 2004).

An example of a diffraction pattern from a b.c.t. colloidal crystal is presented in Fig. 3. The crystal consists of 15 ± 1 hexagonal close-packed layers of silica spheres. The X-ray beam is normal to the hexagonal planes. The reflections are indexed using orthogonal generating vectors of length $b_1 = b_2 = 4\pi/(6^{1/2}a)$ and $b_3 = 2\pi/a$, where a is the nearest-neighbour distance. Here the $\mathbf{b}_3$ vector is parallel to the direction of the applied electric field. Reflections of a b.c.t. crystal can be observed for even values of $(h + k + l)$. For the crystal orientation used here, only the reflections with $h = k$ and even values of l can be seen. The dashed arrows in Fig. 3 point to lines of reflections, which should be absent in a perfect b.c.t. crystal because of the cancellation of the contributions of two

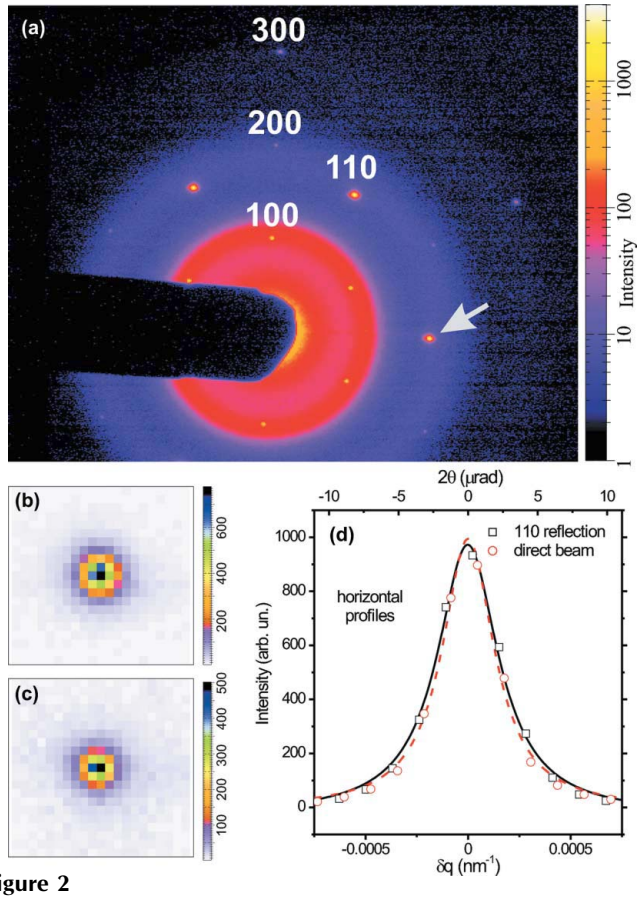

Figure 2
(*a*) Diffraction pattern (1280 × 1024 pixels) from coexisting fluid–wall crystals in a cylindrical capillary with a PMMA hard-sphere colloidal suspension. Exposure time τ = 10 s. Note that the strong 110-class reflections oversaturate the detector here. Panel (*b*) presents a magnification (21 × 21 pixels) of the 110-class reflection marked in (*a*) by a white arrow (taken from a similar pattern but measured with the exposure time of τ = 1 s). For comparison, (*c*) shows a magnified view of the direct beam after removing the beam stop (τ = 1 ms). Note that a linear intensity scale is used in (*b*) and (*c*), and a logarithmic scale in (*a*). In panel (*d*), the squares and circles represent the pixel readings in horizontal slices through the peaks in panels (*b*) and (*c*), respectively. The lines are the Lorentzian fits to the data. The vertical scale for both data sets is slightly readjusted.

subsequent hexagonal layers. Their small but finite intensity can be related to the small number of layers in the crystal and lattice imperfections. The solid arrows point to two of the stronger non-b.c.t. reflections, which also indicate that a small portion of the crystal has changed the stacking from bridge-site to hollow-site. These reflections correspond to the 110-class reflections in Fig. 2(*a*). Their intensity, however, is very much smaller than that of the 002 reflection with the same form factor and, thus, the b.c.t. structure dominates in the crystal.

The smallest diffraction angle of $2\theta_{110}$ = 69 μrad originates from the largest real-space interplanar spacing, which corresponds to the distance between lines of close-packed particles in a hexagonal layer. From the magnitude of the diffraction vector $\mathbf{q}_{110}$ in the pattern in Fig. 3, a value for the d_{110} distance of 1.35 ± 0.04 μm was found. The 3% uncertainty in the absolute value of d_{110} mostly originates from inaccuracy of the q-space calibration. It compares well with d_{110} = 1.32 ± 0.01 μm determined by confocal microscopy. The angular resolution achieved in this experiment allowed us not only to resolve the diffraction pattern at tiny diffraction angles 2θ, but also to detect further details related to the crystal quality. For example, in the crystal used in Fig. 3, the FWHM of the reflections in the radial direction is (4.5–5) × 10^{-4} nm^{-1}, *i.e.* somewhat larger than the width of the instrument resolution function. This means that the crystal possesses a finite spatial extent of positional correlations. Moreover, the diffraction peaks are seen to be broadened in the azimuthal direction, which reveals a mosaic structure of the crystal with a small degree of misorientation between the crystallites. We are currently analysing in more detail the reflection widths of various reflections measured in samples at different stages of the fabrication process of inverted photonic crystals. This further analysis is beyond the scope of this work and will be published elsewhere (Thijssen *et al.*, to be published).

6. Disorder in a crystal of silica spheres

Fig. 4 displays two examples of the diffraction patterns measured from r.h.c.p. crystals of sterically stabilized hard silica spheres (diameter 224 nm, dispersed in cyclohexane). The system is described in more detail by Petukhov *et al.* (2004). The crystals spontaneously formed in the sediment at the bottom of two different flat glass capillaries (4 mm wide, internal path length 0.2 mm). The two patterns in Fig. 4 show Bragg reflections with remarkably different shapes. While panel (*a*) displays (almost) circular symmetric reflections, panel (*b*) has reflections that are strongly spread in the azimuthal direction. It is obvious that the improved resolution is crucial to observe the distinction between the two crystals,

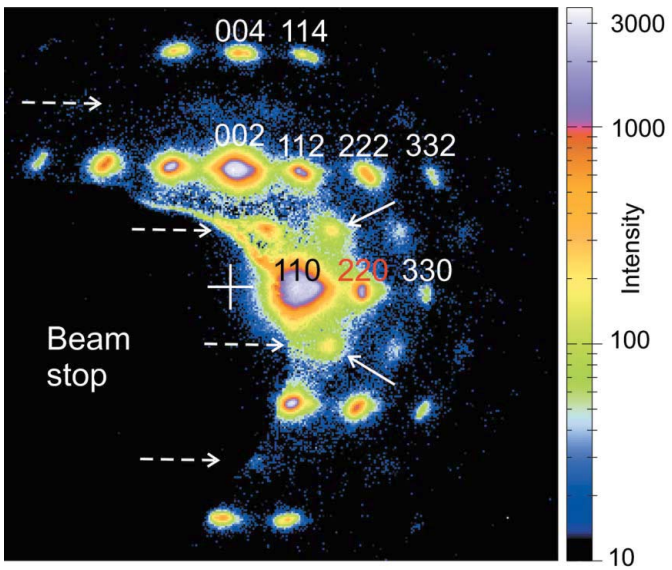

Figure 3
A magnification (300 × 300 pixels) of the central part of the diffraction pattern from a b.c.t. colloidal crystal. The white cross denotes the position of the direct beam, which is behind the beam stop. Note that the 110 and 002 reflections oversaturate the detector and their widths are greatly exaggerated. See text for further details.

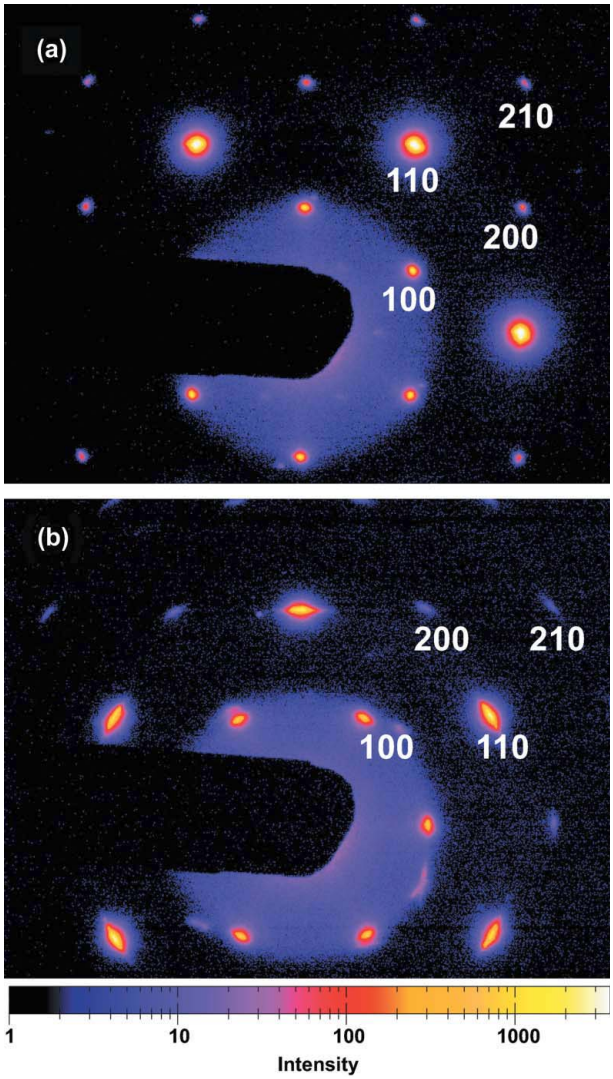

Figure 4
Diffraction patterns from two different crystals of silica hard spheres. Both crystals are oriented such that the X-ray beam is orthogonal to the hexagonal planes. The exposure time $\tau = 10$ s. Note that at this exposure the 100 reflection and, especially, the intense 110 reflection highly oversaturate the detector, so that their widths are greatly exaggerated.

which would not have been possible with the resolution used by Vos *et al.* (1997), van der Kooij *et al.* (2000), Versmold *et al.* (2002) and Petukhov *et al.* (2002).

We have further studied the reflection width $\delta q_{\rm app}$ in the radial direction. For all reflections in Fig. 4(*a*) except the 110 reflection, the apparent width is found to be notably (two to four times) larger than the width of the instrument resolution function Δ determined from the width of the direct beam. Thus, the improved resolution allowed us to determine the intrinsic width of different reflections $\delta q_{\rm intr}$ using equation (2). The result is summarized in Fig. 5 for reflections of different order. Due to very distinct differences in the intensities of the reflections, the intrinsic width δq_{hkl} for different *hkl* reflections is determined from patterns taken with different exposure times τ. For the crystal which yielded the diffraction pattern shown in Fig. 4(*a*), $\tau = 1$, 0.01, 10 and 60 s was used for the 100, 110, 200 and 210 reflections, respectively. For the other crystal,

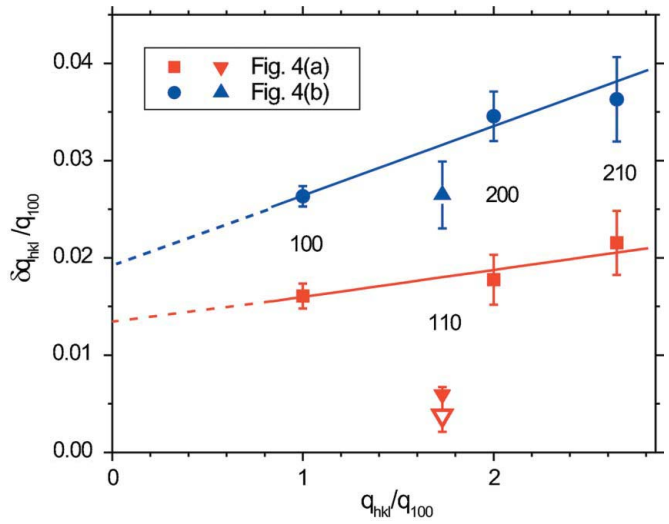

Figure 5
The radial intrinsic width δq_{hkl} of the different-order reflections in the patterns shown in Fig. 4 as a function of the diffraction vector magnitude q_{hkl}. The error bars represent the spread of the values obtained from different reflections of the same class. The lines are the linear fits to the widths of the *hkl* = 100-, 200- and 210-class reflections originating from the Bragg rods induced by the stacking disorder. The values of δq and q_{hkl} on both axes are rescaled to the q value of the lowest order reflection, $q_{100} = 0.0310\ {\rm nm}^{-1}$ and $q_{100} = 0.0309\ {\rm nm}^{-1}$ in Figs. 4(*a*) and 4(*b*), respectively. The filled symbols represent the results obtained from the analysis of the data taken with the CCD detector. The open triangle is the estimate of the upper limit of the width of the 110 reflection of the crystal in Fig. 4(*a*) as obtained with X-ray films (see §7).

which produced the pattern shown in Fig. 4(*b*), the corresponding exposure times were respectively $\tau = 10$, 1, 300 and 300 s. As one can expect, δq_{hkl} in Fig. 4(*b*) is larger than that in Fig. 4(*a*). We also observe a slight increase of the radial width with the reflection order. Surprisingly, a difference in δq_{hkl} is found between the 100, 200 and 210 reflections originating from the Bragg rods, and the 110 reflection originating from the true Bragg spot. This difference in the width is especially pronounced in the case of the crystal yielding the pattern presented in Fig. 4(*a*), where the apparent width δq_{110} of the 110 reflection is still instrument-dominated so that it is difficult to determine its intrinsic width precisely. In the following section we give another estimate of the upper limit of δq_{110} for this crystal.

We propose that the width of the reflections has two components. One component is independent of the diffraction order and can be related to the effect of the size of crystallites Λ in the mosaic constituting the macrocrystal. The other component which increases with increasing q can be induced by second-type disorder (Guinier, 1994). We further assume a simple linear relation

$$\delta q_{hkl} = \delta q_0 + \gamma q_{hkl}. \qquad (3)$$

Using a linear fit to the data, for the reflections originating from the Bragg rods intersected by the Ewald sphere one can estimate δq_0 to be $(4.1 \pm 0.8) \times 10^{-4}\ {\rm nm}^{-1}$ and $(6.0 \pm 0.8) \times 10^{-4}\ {\rm nm}^{-1}$ in the first (Fig. 4*a*) and the second (Fig. 4*b*) crystal, respectively. The typical size of the crystallites can be estimated as $\Lambda = 2\pi B/\delta q_0$, where B is a factor of the order 1, which

depends on the crystal shape. Using $B = 1$ one obtains $\Lambda = 16$ µm and 10 µm, respectively. For the slope γ we find the values of $(3 \pm 2) \times 10^{-3}$ and $(7 \pm 2) \times 10^{-3}$ in the first and the second crystal, respectively.

Unfortunately, due to the limited q range, our current data do not allow us to distinguish the q-dependent and the q-independent components of the width of the true Bragg spots (with $l = 0$ and $h - k$ divisible by 3). A more elaborate experimental study as well as theoretical modelling of the long-range order parameters in colloidal crystals grown from concentrated dispersions is needed and will be performed in the future. However, this example already shows that the improved angular resolution allows us to access novel detailed information on the range of various order parameters in colloidal crystals, including first- and second-type disorder.

7. X-ray film measurement

As shown above, the data measured with the CCD detector had an angular resolution of 4.6 µrad. To test the ultimate limit of the angular resolution of the setup, we also recorded the direct beam and the diffracted beams on high-resolution X-ray-sensitive films. Unfortunately, all the images of the direct beam turned out to be too overexposed. During the experiment, no fast beam shutter was available to ensure a sufficiently short exposure time. Thus, instead of the direct beam, we present in Fig. 6 (inset) an image of one of the 110-class reflections of the r.h.c.p. hard-sphere colloidal crystal (see Fig. 4*a*).

The image on the X-ray film was digitized using an optical microscope (×32 magnification, spatial resolution of 0.5 µm) equipped with a CCD camera. The result was corrected with respect to the blackening curve of the film. A slice through the reflection in the radial direction has an FWHM of less than 6 µm. For our experimental geometry, this corresponds to an apparent radial width of about $\delta q_{\rm app} = 1.2 \times 10^{-4}$ nm^{-1}. Unfortunately, we do not have the information needed to determine the contributions of the instrument resolution and the intrinsic reflection width of the crystal. Nevertheless, the value of 1.2×10^{-4} nm^{-1} sets an upper limit for both of them. The open triangle in Fig. 5 represents the result of this estimate.

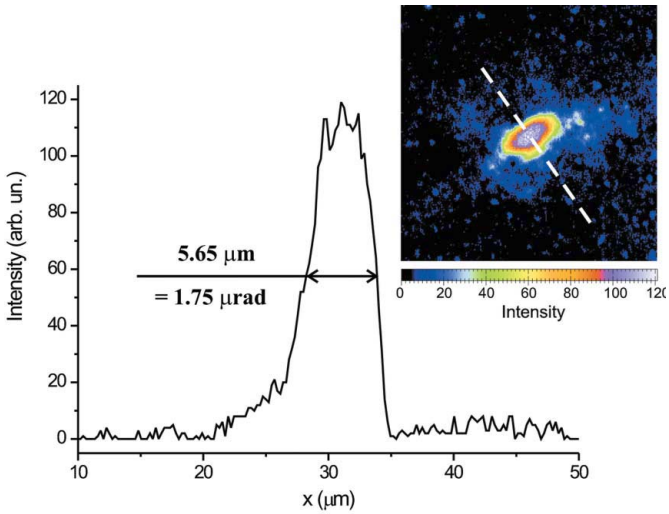

Figure 6
Image of one of the 110-class reflections from the colloidal crystal shown in Fig. 4(*a*) obtained with the high-resolution X-ray film. The X-ray intensities at every pixel are calculated from the film density using the blackening curve. A 50 µm × 50 µm area is presented in the inset. The profile is taken in the radial direction (dashed line in the image).

Thus, our results show that the SAXS scheme with refractive optics at a synchrotron source allows the achievement of an angular resolution that is even higher than that in the data presented in the §§4–6, where the spatial resolution of the CCD detector was the limiting factor. The higher resolution achieved in the X-ray film measurements also revealed that the 110 reflection is slightly broadened in the azimuthal direction. This broadening is practically invisible in Fig. 4(*a*).

8. Concluding remarks

In the present work we have presented a few examples of the application of the ultra-high-resolution SAXS technique to colloidal crystals. It is demonstrated that an angular resolution better than 2 µrad can be achieved using a synchrotron X-ray source and refractive optics for a sample–detector distance of only a few metres. This resolution is about one order of magnitude higher than the resolution of the presently realised USAXS installations exploiting Si-111 and Si-220 Bonse–Hart cameras (Narayanan *et al.*, 2001; Ilavsky *et al.*, 2002). The setup enables fast recording of two-dimensional diffraction data within the (sub)second acquisition time. One has to note, however, that at present the compound refractive lenses have a rather high level of parasitic scattering, which leads to an increase of the scattering background. This might create an obstacle for weakly scattering samples and further improvement of the quality of the lenses is highly desirable.

The breakthrough in terms of the angular resolution to a few microradians makes SAXS a powerful analytical tool which allows detailed quantitative characterization of colloidal crystals. It can provide a clear distinction between the X-ray scattering from a colloidal fluid and the X-ray diffraction from a coexisting small colloidal crystal grown at the capillary wall (§4). Microradian-resolution SAXS is able to provide a detailed structural evaluation of colloidal crystals with particle separations of even larger than 1 µm (§5). The technique can give access to new detailed knowledge on the order parameters, such as the presence of disorder of the second type (§6).

The case of the colloidal photonic crystals is presumably not the only example where improvement of the angular resolution in two-dimensional data acquisition can play an important role. For example, it could be of importance for biological objects with large-scale organization, such as in muscles (Linari *et al.*, 2000; Yagi & Inoue, 2003; Reconditi *et al.*, 2004). Microradian resolution may be needed to enlarge the unit-cell size accessible to protein crystallography, in order to study

large protein complexes such as viruses (Grimes & Stuart, 1998).

It is our pleasure to thank Federico Zontone, Henri Gleyzolle, Patrick Feder, Andrei Fluerasu and Anders Madsen for their excellent support, and Patrick Davidson, Theyencheri Narayanan, Henk Lekkerkerker and Gert Jan Vroege for stimulating discussions. Marc Diot and Cyril Ponchut are acknowledged for providing the detector. ESRF is thanked for granting us the beam time. We also appreciate the constructive criticism of the referees.

References

Anderson, V. & Lekkerkerker, H. N. W. (2002). *Nature (London)*, **416**, 811–815.
Astratov, V. N., Adawi, A. M., Fricker, S., Skolnick, M. S., Whittaker, D. M. & Pusey P. N. (2002). *Phys. Rev. B*, **66**, 165215.
Auer, S. & Frenkel, D. (2001). *Nature (London)*, **409**, 1020–1023.
Blanco, A., Chomski, E., Grabtchak, S., Ibisate, M., John, S., Leonard, S. W., Lopez, C., Meseguer, F., Miguez, H., Mondia, J. P., Ozin, G. A., Toader, O. & van Driel, H. M. (2000). *Nature (London)*, **405**, 437–440.
Bonse, U. & Hart, M. (1966). *Z. Phys.* **189**, 151–162.
Dassanayake, U., Fraden, S. & van Blaaderen, A. (2000). *J. Chem. Phys.* **112**, 3851–3858.
Dogic, Z. & Fraden, S. (1997). *Phys. Rev. Lett.* **78**, 2417–2420.
Drakopoulos, M., Snigirev, A., Snigireva, I. & Schilling, J. (2005). *Appl. Phys. Lett.* **86**, 014102.
Freund, A. K. (1998). *Synchrotron X-ray Beam Optics*, in *Complementarity Between Neutron and Synchrotron X-ray Scattering*, edited by A. Furrer, p. 329. Singapore: World Scientific.
Grimes, J. M. & Stuart, D. I. (1998). *Nature Struct. Biol.* **5**, 630–634.
Guinier, A. (1994). *X-ray Diffraction: In Crystals, Imperfect Crystals and Amorphous Bodies.* New York: Dover Publications.
Harada, T., Matsuoka, H., Ikeda, T. & Yamaoka, H. (2000). *Colloids Surf. A*, **174**, 79–98.
Harland, J. L. & van Megen, W. (1997). *Phys. Rev. E*, **55**, 3054–3067.
Joannopoulos, J. D., Meade R. D. & Winn, J. N. (1995). *Photonic Crystals*. Princeton University Press.
Ilavsky, J., Allen, A. J., Long, G. G. & Jemain, P. R. (2002). *Rev. Sci. Instrum.* **73**, 1660–1662.
Imhof, A. (2003). *Nanoscale Materials*, edited by L. M. Liz-Marzan & P. V. Kamat, pp. 423–454. Boston: Kluwer Academic.
Kegel, W. K. & Dhont, J. K. G. (2000). *J. Chem. Phys.* **112**, 3431–3436.
Kohn, V., Snigireva, I. & Snigirev, A. (2003). *Opt. Commun.* **216**, 247–260.
Kooij, F. M. van der, Kassapidou, K. & Lekkerkerker, H. N. W. (2000). *Nature (London)*, **406**, 868–871.
Lemaire, B. J., Davidson, P., Panine, P. & Jolivet, J. P. (2004). *Phys. Rev. Lett.* **93**, 267801.
Linari, M., Piazzesi, G., Dobbie, I., Koubassova, N., Reconditi, M., Narayanan, T., Diat, O., Irving, M. & Lombardi, V. (2000). *Proc. Natl Acad. Sci.* **97**, 7226–7231.
Megens, M. & Vos, W. L. (2001). *Phys. Rev. Lett.* **86**, 4855–4858.
Narayanan, T., Diat, O. & Boesecke, P. (2001). *Nucl. Instrum. Methods*, **467**, 1005–1009.
Petukhov, A. V., Aarts, D. G. A. L., Dolbnya, I. P., de Hoog, E. H. A., Kassapidou, K., Vroege, G. J., Bras, W. & Lekkerkerker, H. N. W. (2002). *Phys. Rev. Lett.* **88**, 208301.
Petukhov, A. V., Dolbnya, I. P., Aarts, D. G. A. L. & Vroege, G. J. (2004). *Phys. Rev. E*, **69**, 031405.
Petukhov, A. V., Dolbnya, I. P., Aarts, D. G. A. L., Vroege, G. J. & Lekkerkerker, H. N. W. (2003). *Phys. Rev. Lett.* **90**, 028304.
Petukhov, A. V., van der Beek, D., Dullens, R. P. A., Dolbnya, I. P., Vroege, G. J. & Lekkerkerker, H. N. W. (2005). *Phys. Rev. Lett.* **95**, 077801.
Pusey, P. N. & van Megen, W. (1986). *Nature (London)*, **320**, 340–342.
Pusey, P. N., van Megen, W., Barlett, P., Ackerson, B. J., Parity, J. G. & Underwood, S. M. (1989). *Phys. Rev. Lett.* **63**, 2753–2756.
Reconditi, M., Linari, M., Lucil, L., Stewart, A., Sun, Y.-B., Boesecke, P., Narayanan, T., Fischetti, R. F., Irving, T., Piazzesi, G., Irving, M. & Lombardi, V. (2004). *Nature (London)*, **428**, 578–581.
Rengarajan, R., Mittleman, D., Rich, Ch. & Colvin, V. (2005). *Phys. Rev. E*, **71**, 016615.
Schall, P., Cohen, I., Weitz, D. A. & Spaepen, F. (2004). *Science*, **305**, 1944–1948.
Sinha, S. K., Tolan, M. & Gibaud, A. (1998). *Phys. Rev. B*, **57**, 2740–2758.
Sirota, E. B., Ou-Yang, H. D., Sinha, S. K., Chaikin, P. M., Axe, J. D. & Fujii, Y. (1989). *Phys. Rev. Lett.* **62**, 1524–1527.
Snigirev, A., Kohn, V., Snigireva, I. & Lengeler, B. (1996). *Nature (London)*, **384**, 49–51.
Veen, F. van der & Pfeiffer, F. (2004). *J. Phys. Condens. Matter*, **16**, 5003–5030.
Versmold, H., Musa, S. & Bierbaum, A. (2002). *J. Chem. Phys.* **116**, 2658–2662.
Vlasov, Y. A., Bo, X. Z., Sturm, J. C. & Norris, D. J. (2001). *Nature (London)*, **414**, 289–293.
Vos, W. L., Megens, M., van Kats, C. M. & Boesecke, P. (1997). *Langmuir*, **13**, 6004–6008.
Yagi, N. & Inoue, K. (2003). *J. Appl. Cryst.* **36**, 783–786.
Yethiraj, A. & van Blaaderen, A. (2003). *Nature (London)*, **421**, 513–517.
Yethiraj, A., Thijssen, J. H. J., Wouterse, A. & van Blaaderen, A. (2004). *Adv. Mater.* **16**, 596–600.
Zhu, J., Li, R., Rogers, W., Meyer, W., Ottewill, R. H., STS-73 Space Shuttle Crew, Russel, W. B. & Chaikin, P. M. (1997). *Nature (London)*, **387**, 883–885.